Proceedings of the ASME Turbo Expo 2023
Turbomachinery Technical Conference and Exposition
GT2023
June 26–30, 2023, Boston, Massachusetts

GT2023-101735

MODEL PREDICTIVE CONTROL STRATEGIES FOR TURBINE ELECTRIFIED ENERGY MANAGEMENT

Elyse D. Hill[1,*], Aria E. Amthor[2], Donald I. Soloway[3], Donald L. Simon[2], Joseph W. Connolly[2,*]

[1]NASA Postdoctoral Program Fellow, NASA Glenn Research Center, Cleveland, OH
[2]Control Systems Engineer, NASA Glenn Research Center, Cleveland, OH
[3]Control Systems Engineer, NASA Ames Research Center, Moffett Field, CA

ABSTRACT

The increasing electrification of aircraft propulsion systems is leading to new control architectures being developed to address integration between electric machines and gas-based turbine engines. For hybrid-electric propulsion systems, current conceptual architectures often couple electric machines with the shafts of gas turbine engines and introduce energy storage. Leveraging the electrical power system of hybridized engines, Turbine Electrified Energy Management (TEEM) is a recent control approach that improves transient operability in an effort to enable more efficient and lighter weight turbomachinery. This study seeks to expand TEEM's application beyond traditional proportional-integral (PI) control by presenting linear model predictive control (MPC) schemes to execute the TEEM concept. Through constraint selection and cost function design, transient operability goals for TEEM are considered with no external logic or saturation. Unique to the designs are the use of a washout filter, which simplifies transient detection and motor activation logic. The proposed architectures are implemented with both centralized MPC and distributed MPC approaches, and comparisons are drawn to a benchmark PI controller simulated on a nonlinear turbofan engine model at one ground condition and one cruise condition. Performance is evaluated using compressor maps, stall margin performance, and two novel metrics: transient stack usage and transient excursion integral. Results reveal the linear MPC scheme performs comparably to the baseline controller and can be implemented in at least two distinct configurations with potential for further modifications, thus establishing the groundwork for future investigations.

Keywords: model predictive control, linear control, turbomachinery

NOMENCLATURE

Roman letters

A	System state matrix.
AC	Alternating current.
a	Washout filter variable for exponential decay.
B	System input matrix.
C	System output matrix.
D	System feedforward matrix.
DC	Direct current.
J	Open-loop cost function.
l	Stage cost function.
M	Motor torque.
m	Number of control inputs.
N	Shaft speed.
n	Number of states.
PR	Pressure ratio.
Q	Output weight matrix.
r	Number of outputs.
R	Control weight matrix.
SM	Stall margin.
t	Simulation time.
T	Time horizon.
T_s	Sampling time.
T_u	Time horizon for inputs.
TEI	Transient excursion integral.
TSU	Transient stack usage.
u	System control input.
$\mathcal{U}$	System control constraint set.
VAFN	Variable area fan nozzle.
VBV	Variable bleed valve.
W_c	Corrected fuel flow.
W_f	Fuel flow variable.
x	System states.
$\mathcal{X}$	System state constraint set.
y	System outputs.
$\mathcal{Y}$	System output constraint set.
$\mathcal{Y}_f$	System terminal constraint set.

*Corresponding author: elyse.d.hill@nasa.gov, joseph.w.connolly@nasa.gov

Greek letters

Δ	Change between time steps.
δ	System perturbation variable.
Ω	Augmented input vector.
ϕ	Acceleration threshold value.
τ	Time sequence over time horizon.

Superscripts and subscripts

$\cdot^*$	Denotes optimal solution.
$\tilde{\cdot}$	Denotes error.
$\cdot_0$	Denotes initial variable value.
$\cdot_e$	Denotes belonging to engine subsystem.
$\cdot_f$	Denotes relation to fuel.
$\cdot_{fan}$	Denotes relation to fan variable.
$\cdot_{HPS}$	Denotes relation to high pressure shaft.
$\cdot_i$	Denotes index placeholder.
$\cdot_{lb}$	Denotes lower bound.
$\cdot_{LPS}$	Denotes relation to low pressure shaft.
$\cdot_p$	Denotes belonging to power subsystem.
$\cdot_{SS}$	Denotes operation at engine steady-state.
$\cdot_{stall}$	Denotes operation at engine stall.
$\cdot_{TEEM}$	Denotes relation to TEEM implementation.
$\cdot_{trim}$	Denotes trim value.
$\cdot_{ub}$	Denotes upper bound.
$\cdot_{washout}$	Denotes relation to washout filter.

1. INTRODUCTION

According to NASA's Aeronautics Research Mission Directorate, the future of aeronautics research lies in developing and implementing strategies that enable safe, affordable, efficient, and autonomous aircraft [1]. This includes the development and testing of technologies that enable the use of electrified aircraft propulsion (EAP) systems as alternatives to solely gas-based aircraft propulsion. Of the variety of EAP systems, hybrid-electric architectures are of distinct focus. Here, there are efforts to exploit electric system components to supplement traditional gas-based propulsion for improving overall propulsion system and vehicle efficiency. This involves the use of electrical components to contribute additional propulsive and aerodynamic benefits while adhering to thermal management constraints [2–6].

Turbine Electrified Energy Management (TEEM) is a control strategy for hybrid-electric systems that takes advantage of the coupling between electric power system components and gas turbine engine shafts to alleviate engine design constraints through improved system operability [7]. Specifically, electric machines (EMs) are used during acceleration and deceleration to inject or extract power from engine shafts. As a result, during transients the engine operates closer to its steady-state behavior, thus reducing excursions towards stall or surge. The feasibility and effectiveness of the method was previously well demonstrated in [7–12], where compressor susceptibility to stall and surge during engine transients was successfully mitigated upon application of TEEM. While effective, to date TEEM has only been applied with simplified, decentralized control architectures, such as open-loop schedule-based control or closed-loop scheduled proportional-integral (PI) control [8, 13]. In decentralized control, multiple local controllers address the control goals of individual subsystems without knowledge or consideration of other subsystem interconnections and priorities. The natural drawbacks to these designs include the need for additional limit logic to account for system constraints, the inability to consider subsystem interactions holistically, and the challenge of defining logic over a full system operating envelope.

The shortcomings can be overcome with control designs that account for multiple objectives, constraints, and system interactions. These elements are features of model predictive control (MPC), an advanced, optimal control technique that constructs an optimal control effort over a time horizon for a system with respect to state and input constraints [14]. Known for its capability to control complex, multivariable systems with minimal conceptual complexity, MPC has been increasingly used in a number of EAP applications [15–19], where it demonstrates the ability to handle various system objectives, exploit look-ahead information, and effectively manage relations between turbomachinery and electric subsystems. Both centralized MPC (CMPC) and distributed MPC (DMPC) architectures have been explored and have proven effective [20–23]. In the centralized design, one MPC possesses complete system knowledge and executes system-wide control actions while in the distributed design two or more MPCs with partial system knowledge collaborate to determine local control actions.

In this paper, an application of TEEM is proposed using CMPC. The goal of the design is to consolidate the decentralized architecture into one controller, such that the drawbacks of the traditional approaches are avoided. The constrained optimization allows the goals of TEEM to be explicitly built into the MPC cost function and removes the need for separate control logic, including limit protection logic. The architecture uses a piece-wise linear dynamic system to represent a nonlinear engine model, allowing all subsystem interactions to be considered. Novel to the design is the use of a time-domain washout filter that regulates EM torques to zero during steady-state operation. Motivated by findings in [22] and discussions in [24], a DMPC architecture is developed alongside the CMPC to explore advantages and disadvantages in MPC approaches. The proposed schemes are simulated with a nonlinear engine model in two case studies with and without TEEM implemented. The controllers are also compared to a benchmark closed-loop, scheduled PI controller developed in [8]. Performance is evaluated using stall margins, low and high pressure compressor map data, and two numeric metrics that will be described in Section 2.

The remainder of this paper is organized as follows: Section 2 reviews the nonlinear engine model and its piece-wise linear representation, followed by a review of the goals of TEEM. Section 3 presents the proposed MPC control architectures and Section 4 discusses the simulation results. Finally, the paper is concluded in Section 5.

2. OVERVIEW OF ENGINE MODEL AND TEEM

2.1 AGTF30 Engine Model

The Advanced Geared Turbofan 30,000lbf (AGTF30) engine is a conceptual turbofan engine able to produce 30klbf of thrust at sea-level static conditions [25]. The engine is modeled in MATLAB/Simulink using the Toolbox for Modeling and Analysis of Thermodynamic Systems (T-MATS) [26]. An electrified

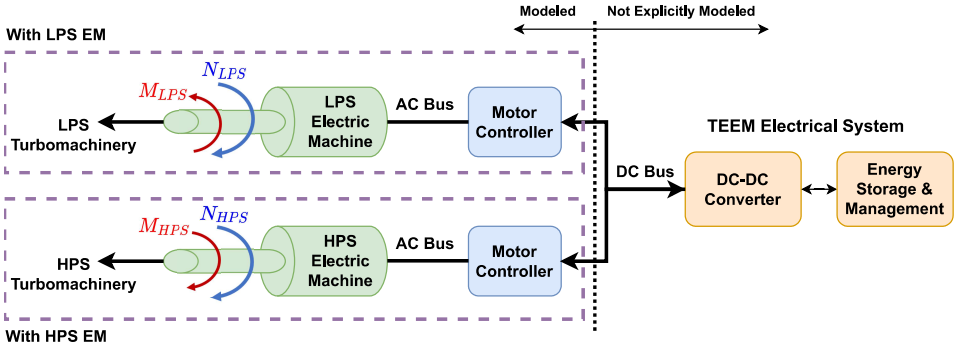

FIGURE 1: TEEM ELECTRICAL SYSTEM ARCHITECTURE; REPRODUCED FROM [8].

version of the AGTF30 developed in [9] is used in this paper. This model uses the Electrical Modeling and Thermal Analysis Toolbox (EMTAT) [27] to mathematically represent the electric motors/generators and associated power systems needed to apply TEEM, illustrated at a high-level in Fig. 1. For the control design, the nonlinear dynamics of the AGTF30 are represented by a piece-wise linear model with each linearization at specific operating points denoted by combinations of altitude (Alt), Mach number (MN), and power lever angle (PLA). The linear dynamic system is represented as follows:

$$\delta\dot{x}(t) = A\delta x(t) + B\delta u(t) \tag{1}$$
$$\delta y(t) = C\delta x(t) + D\delta u(t) \tag{2}$$

where $x(t) \in \mathbb{R}^n$ is the state vector, $u(t) \in \mathbb{R}^m$ is the input vector, $y(t) \in \mathbb{R}^r$ is the output vector, and A, B, C and D are the dynamic system state space matrices. The terms δx, δu, and δy are defined as:

$$\delta x(t) = x(t) - x_{trim}(t) \tag{3a}$$
$$\delta u(t) = u(t) - u_{trim}(t) \tag{3b}$$
$$\delta y(t) = y(t) - y_{trim}(t) \tag{3c}$$

where the subscript $\cdot_{trim}$ represents the value of the state, input, or output vectors when the engine is at steady-state for a given operating condition. The states, inputs, and outputs for the electrified AGTF30 system in this study are:

$$x = \begin{bmatrix} N_{LPS} & N_{HPS} \end{bmatrix}^T \tag{4}$$
$$u = \begin{bmatrix} W_f & M_{LPS} & M_{HPS} & VAFN & VBV \end{bmatrix}^T \tag{5}$$
$$y = \begin{bmatrix} N_{fan} & N_{HPS} & SM_{LPC} & SM_{HPC} \end{bmatrix}^T \tag{6}$$

Equation (4) denotes the speeds of the low and high pressure shafts (LPS, HPS). Equation (5) denotes the fuel flow rate, low and high pressure shaft motor torques, variable area fan nozzle (VAFN) area, and variable bleed valve (VBV) setting. Finally, Eq. (6) denotes the fan speed, high pressure shaft speed, and low and high pressure compressor (LPC, HPC) stall margins (SMs). Note that for the AGTF30 system, the fan shaft and LPS are related by a gear ratio expressed as $N_{LPS} = 3.1N_{fan}$. Also note that while stall margin cannot be directly measured, the AGTF30 can approximate the value permitting its presence in the output vector as a variable of interest. In this study, stall margin is used solely for analysis rather than control purposes.

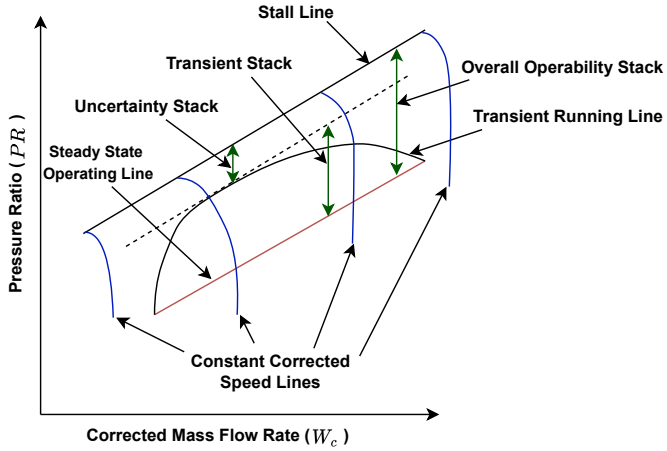

FIGURE 2: ILLUSTRATION OF TEEM CONCEPT; REPRODUCED FROM [28].

2.2 Turbine Electrified Energy Management

The TEEM concept was developed as an operability technology and can be used to accomplish several goals: improving transient stability margins, expanding engine operating range, reducing engine design constraints, and eliminating stability bleeds [8, 9]. This study only considers stability margin improvement, narrowing TEEM's goal to managing transient operability, or the susceptibility of the engine compressors to stall. TEEM's effectiveness can be evaluated both graphically, using compressor maps, and numerically, using three metrics: compressor stall margin, transient stack usage (TSU), and transient excursion integral (TEI). Engine compressor maps plot pressure ratio (PR) versus corrected airflow and indicate engine operation between stall and choke. Successful implementation of TEEM shifts the transient running line, shown in Fig. 2, away from the stall line and towards the steady-state operating line. This increases compressor stall margin during transients and allows the engine to operate closer to steady-state conditions. Both TSU and TEI, developed in [13] and illustrated in Fig. 2, are performance measures defined as:

$$TSU = \max\left(\frac{PR - PR_{SS}}{PR_{stall} - PR_{SS}}\right) \times 100\% \tag{7}$$

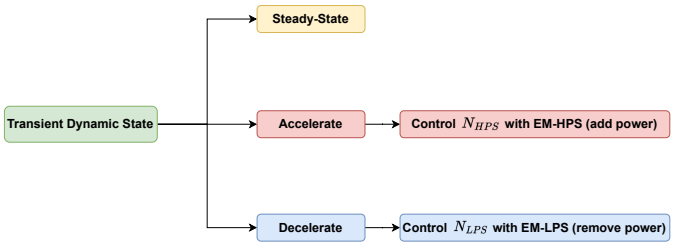

FIGURE 3: DUAL-SPOOL TEEM CONFIGURATION.

$$TEI = \int \left| \frac{PR - PR_{SS}}{PR_{SS}} \right| dW_c \tag{8}$$

where the subscript $\cdot_{stall}$ represents operation at engine stall and the subscript $\cdot_{SS}$ represents engine operation at steady-state. TSU measures the maximum percent of the overall operability stack used during a transient. As seen in Fig. 2, the overall operability stack represents the space between the steady-state operating line and the stall line. It encompasses both uncertainty stack, which accounts for factors such as engine to engine variation and engine degradation, and transient stack, which is the variation experienced through engine transients. With this measure, TSU indicates the closest the transient running line veered towards the stall line by defining the ratio of transient stack to overall operability stack. TEI measures the deviation of the transient running line from the steady-state operating line and is representative of the area between both lines which are shown in Fig. 2. Successful application of TEEM is expected to reduce the values of TEI and TSU. Reference [8] outlined several control configurations characterized by the existence and use of electric machines on each of the engine spools for the benchmark TEEM-based PI architecture. For the purposes of this study, only the dual-spool TEEM configuration is used, as displayed in Fig. 3, in which motors on both LPS and HPS are used for torque subtraction and addition, respectively. In the TEEM-based PI, the transient dynamic state is identified using additional control logic that determines acceleration or deceleration based on the tracking error of the active fuel flow controller or the acceleration of the fan speed. The active fuel flow controller can represent a control limit constraint related to temperature, pressure, or shaft speed. This transient on/off logic allows TEEM to activate commands to the HPS and LPS EMs during transients and to deactivate those commands during steady-state operation. Contrary to the studies in [8] where power requested by the EMs is absorbed or supplied by the energy storage system, no energy storage capacity regulation is considered in this paper. Figure 1 reflects this consideration by indicating the explicitly modeled portions of the TEEM electrical system for this work.

3. CONTROLLER DESIGN

This section describes the proposed MPC architectures, which are shown integrated at a high level in Fig. 4. The energy storage sub-system is listed but not considered in the controller design. Both the DMPC and CMPC architectures can be substituted into the controller block depending on the configuration.

Considering Eqs. (1)-(2), a linear MPC optimal control problem can be stated as:

Problem 1 (General Optimal Control Problem)

$$\begin{aligned}
\min_{u} \quad & J(\delta y, \delta u) = \int_{t}^{t+T} l(\delta y(\tau), \delta u(\tau)) d\tau && (9a)\\
\textit{subject to} \quad & \delta y(t) = \delta y_0 && (9b)\\
& \delta \dot{x}(\tau) = A\delta x(\tau) + B\delta u(\tau), && (9c)\\
& \delta y(\tau) = C\delta x(\tau) + D\delta u(\tau), && (9d)\\
& \delta x(\tau) \in \mathcal{X} - x_{trim}, && (9e)\\
& \delta u(\tau) \in \mathcal{U} - u_{trim}, && (9f)\\
& \delta y(\tau) \in \mathcal{Y} - y_{trim}, && (9g)\\
& \delta y(t+T) \in \mathcal{Y}_f - y_{trim}, && (9h)\\
& \tau \in [t, t+T]
\end{aligned}$$

where T is the length of the time horizon, τ is the time variable along the horizon, y_0 is the initial condition of the output variable, and $\mathcal{X}, \mathcal{U}, \mathcal{Y}$ and $\mathcal{Y}_f$ are the respective state, input, output, and terminal constraint sets. The term $l(\cdot)$ is the quadratic stage cost represented generically by $||\cdot||^2_\Pi$, which is the Euclidean norm weighted by a symmetric, positive-definite matrix Π. Note that although a terminal cost is omitted in Problem 1, the presence of the terminal constraint in Eq. (9h) is enough to ensure closed-loop stability [14]. The output of Eq. (9) is the optimal open-loop input sequence over the horizon $u^*(t)$, of which only the first instance is applied to the closed-loop system.

The main control goal of TEEM is tracking the steady-state reference points x_{SS} during transients. These reference points are determined by the steady-state performance of the AGTF30 at operating conditions designated by altitude, Mach number, and the fuel flow rate command. Additionally, tracking of x_{SS} is supplemented by the activation of EMs during transients. Thus, the on/off logic described in Section 2.2 is used in two ways in the TEEM-based PI: (1) to cue steady-state reference tracking and (2) to cue motor activation. In this study, a primary design goal is to permit the MPC flexibility in determining when to activate the motors i.e. to remove the on/off logic to cue motor activation. This limits the use of transient detection logic to tracking x_{SS}, which is translated into the following piece-wise logic:

$$\tilde{y}_{TEEM} = \begin{cases} N_{LPS} - N_{LPS,SS} & if \quad \dot{N}_{fan} < -\phi \\ N_{HPS} - N_{HPS,SS} & if \quad \dot{N}_{fan} > \phi \end{cases} \tag{10}$$

where $\tilde{\cdot}$ represents an error, $\dot{N}_{fan}$ is the acceleration of the fan, and ϕ is a user-defined acceleration threshold value. It is clear from Eq. (10), that based on the value of ϕ, only one of the steady-state setpoints is represented in $\tilde{y}_{TEEM}$ at a time. Note that these goals are not activated during steady-state. The MPC architecture circumvents transient indication for the motors by using a washout filter. A washout filter is a type of high-pass frequency filter that aids in penalizing DC gain and removing actuator drift [29]. The filter is converted to the time domain and its dynamics inverted to yield the following:

$$(-ae^{-at})^{-1} \tag{11}$$

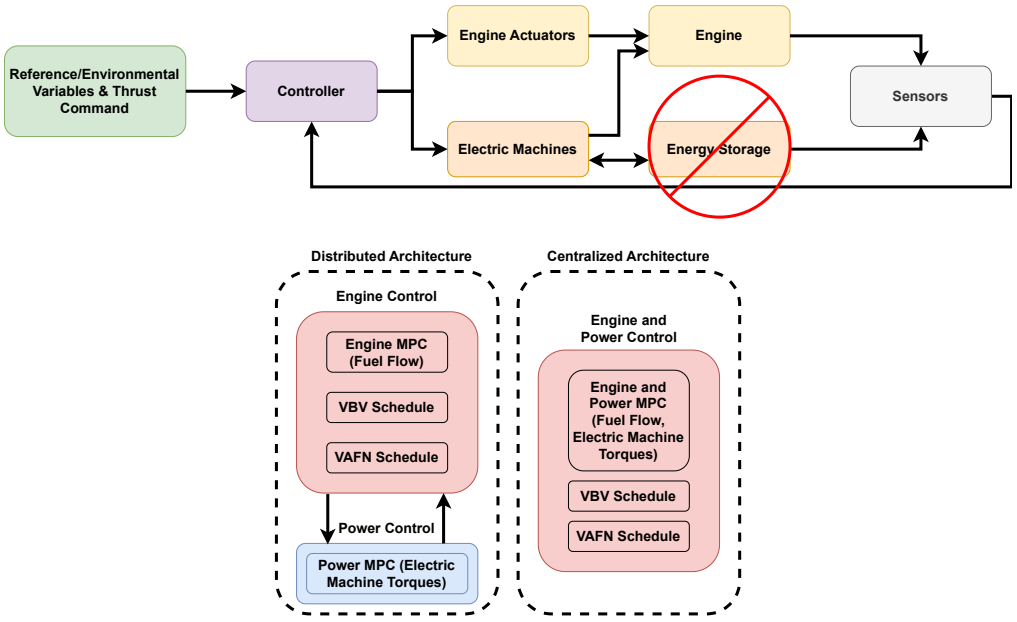

FIGURE 4: PROPOSED CONTROLLER ARCHITECTURE.

where $a \geq 0$ and is selected to control the exponential decay of the function. Multiplying Eq. (11) by the motor inputs yields:

$$u_{washout} = (-ae^{-at})^{-1}[M_{LPS} \quad M_{HPS}]^T \tag{12}$$

Equation (12) keeps the EM torques near zero at steady-state and allows the user to determine via a how quickly the motors return to zero. Incorporating Eq. (12) as a quadratic cost in the stage cost $l(\cdot)$ produces:

$$||u_{washout}||^2_{R_{washout}} \tag{13}$$

where the values of $R_{washout}$ are tuned to influence the magnitude of the motor response. For the TEEM-based MPC, Eqs. (10) and (12) represent the desired transient response denoted by the transient on/off logic in the TEEM-based PI of [8]. While both architectures require an indicator to track steady-state setpoints, the PI requires an indicator for motor activation where the MPC does not as a result of implementing the washout filter. In this study, both centralized and distributed MPCs are constructed for use with TEEM. In the MPCs, both VAFN and VBV are externally scheduled rather than decision variables. This is done to provide a fair comparison with the baseline PI scheme. The PI scheme uses individual PIs to determine W_f, M_{LPS}, and M_{HPS} and open-loop schedules for VAFN and VBV. As a result, the control vector is reduced to $u = [W_f \quad M_{LPS} \quad M_{HPS}]^T$. The optimal control problem for CMPC is similar to Problem 1:

Problem 2 (Centralized MPC Optimal Control Problem)

$$\begin{aligned}
\min_{u} \quad & J(\delta y, \delta u) && (14a)\\
\textit{subject to} \quad & \delta y(t) = \delta y_0 && (14b)\\
& \delta \dot{x}(\tau) = A\delta x(\tau) + B\delta\Omega(\tau), && (14c)\\
& \delta y(\tau) = C\delta x(\tau) + D\delta\Omega(\tau), && (14d)\\
& \delta x(\tau) \in \mathcal{X} - x_{trim}, && (14e)\\
& \delta\Omega(\tau) \in \mathcal{U} - u_{trim}, && (14f)\\
& \delta y(\tau) \in \mathcal{Y} - y_{trim}, && (14g)\\
& \delta y(t+T) \in \mathcal{Y}_f - y_{trim}, && (14h)\\
& \tau \in [t, t+T]
\end{aligned}$$

where the open-loop cost function is:

$$\begin{aligned}
J(\delta y, \delta u) = & \int_t^{t+T} l(\delta\tilde{y}(\tau))d\tau \\
& + \int_t^{t+T_u} l(\Delta u(\tau), \delta u_{washout}(\tau))d\tau
\end{aligned} \tag{15}$$

In (15), the variable $T_u \leq T$ is a shortened time horizon for the control inputs and the stage costs are:

$$l(\delta\tilde{y}(\tau)) = ||\delta\tilde{y}||^2_Q \tag{16}$$

$$l(\Delta u(\tau), \delta u_{washout}(\tau)) = ||\Delta u||^2_R + ||\delta u_{washout}||^2_{R_{washout}} \tag{17}$$

where the tracking error is $\tilde{y} = [N_{fan} - N_{fan,ref} \quad \tilde{y}_{TEEM}]^T$ and where $\Delta u = \delta u(\tau) - \delta u(\tau - T_s)$ with sampling time T_s. To avoid restructuring the state-space model to account for the reduced control vector $u = [W_f \quad M_{LPS} \quad M_{HPS}]^T$, an augmented input vector Ω is introduced. The term Ω is a vector made up of the decision variables (fuel flow and EM torques) as well as the scheduled inputs (VBV and VAFN) described as:

$$\Omega(\tau) = [W_f(\tau) \quad M_{LPS}(\tau) \quad M_{HPS}(\tau) \quad VAFN(t) \quad VBV(t)] \tag{18}$$

The augmented input allows the CMPC to maintain complete system knowledge to make its decisions, eliminating potential information loss that would have resulted from reducing the state-space model to a three input system. During execution, the decision variable inputs $\Omega(\tau)$ are minimized over the horizon, while

the remaining inputs $\Omega(t)$ are values from the initial time instant held constant over the horizon. For the case of Problem 2, only the externally scheduled variables are required to be held constant. This "constant-hold" approach is not uncommon in MPC applications and was deemed acceptable at small timescales, as information loss is minimal.

In the DMPC approach, two MPCs are employed, responsible for controlling the engine (W_f) and power (M_{LPS}, M_{HPS}) control inputs respectively. The DMPC optimal control problem is stated as:

Problem 3 (Distributed MPC Optimal Control Problem)

$$\begin{aligned}
\min_{u_i} \quad & J_i(\delta y_i, \delta u_i) && (19a)\\
\textit{subject to} \quad & \delta y(t) = \delta y_0 && (19b)\\
& \delta \dot{x}(\tau) = A\delta x(\tau) + B\delta\Omega_i(\tau), && (19c)\\
& \delta y(\tau) = C\delta x(\tau) + D\delta\Omega_i(\tau), && (19d)\\
& \delta x(\tau) \in \mathcal{X} - x_{trim}, && (19e)\\
& \delta\Omega_i(\tau) \in \mathcal{U}_i - u_{trim,i}, && (19f)\\
& \delta y(\tau) \in \mathcal{Y} - y_{trim}, && (19g)\\
& \delta y(t+T) \in \mathcal{Y}_f - y_{trim}, && (19h)\\
& \tau \in [t, t+T]
\end{aligned}$$

where the subscript $i \in e, p$ indicates variables belonging to the engine or power subsystem and the augmented input vector for the subsystems are:

$$\Omega_e(\tau) = [W_f(\tau) \quad M_{LPS}(t) \quad M_{HPS}(t) \quad VAFN(t) \quad VBV(t)] \tag{20}$$

$$\Omega_p(\tau) = [W_f(t) \quad M_{LPS}(\tau) \quad M_{HPS}(\tau) \quad VAFN(t) \quad VBV(t)] \tag{21}$$

Specifically, the engine and power cost functions are:

$$\begin{aligned}
J_e(\delta y_e, \delta u_e) = &\int_t^{t+T} l(\delta\tilde{y}_e(\tau))d\tau \\
&+ \int_t^{t+T_u} l(\Delta u_e(\tau))d\tau
\end{aligned} \tag{22}$$

$$\begin{aligned}
J_p(\delta y_p, \delta u_p) = &\int_t^{t+T} l(\delta\tilde{y}_p(\tau))d\tau \\
&+ \int_t^{t+T_u} l(\Delta u_p(\tau), \delta u_{washout}(\tau))d\tau
\end{aligned} \tag{23}$$

where $\tilde{y}_e = \tilde{y}_{N_{fan}}$, $\Delta u_e = \Delta u_{W_f}$, $\tilde{y}_p = \tilde{y}_{TEEM}$, and $\Delta u_p = [\Delta u_{M_{LPS}} \quad \Delta u_{M_{HPS}}]^T$. The stage costs for the engine and power MPCs are:

$$l(\delta\tilde{y}_e(\tau)) = ||\delta\tilde{y}_e||^2_{Q_e} \tag{24}$$

$$l(\Delta u_e(\tau)) = ||\Delta u_e||^2_{R_e} \tag{25}$$

$$l(\delta\tilde{y}_p(\tau)) = ||\delta\tilde{y}_p||^2_{Q_p} \tag{26}$$

$$l(\Delta u_p(\tau), \delta u_{washout}(\tau)) = ||\Delta u_p||^2_{R_p} + ||\delta u_{washout}||^2_{R_{washout}} \tag{27}$$

TABLE 1: SYSTEM PARAMETERS

Shared Parameters	
Parameter	Value
ϕ	0.025
a	1
Centralized MPC Parameters	
Parameter	Value
R^{80}_{ground}	$diag(1.09\times10^6 \quad 0.01 \quad 0.01)$
R^{80}_{cruise}	$diag(6.80\times10^5 \quad 0.01 \quad 0.01)$
R^{48}_{ground}	$diag(1.00\times10^6 \quad 0.01 \quad 0.01)$
R^{48}_{cruise}	$diag(9.85\times10^6 \quad 0.01 \quad 0.01)$
$R_{washout,ground}$	$diag(1.50\times10^{-6} \quad 4.09\times10^{-5})$
$R_{washout,cruise}$	$diag(4.09\times10^{-6} \quad 2.67\times10^{-5})$
Q	$diag(1 \quad 0.001 \quad 0.001)$
Distributed MPC Parameters	
Parameter	Value
$R^{80}_{e,ground}$	1.14×10^6
$R^{80}_{e,cruise}$	6.80×10^6
$R^{48}_{e,ground}$	2.00×10^6
$R^{48}_{e,cruise}$	1.35×10^7
R_p	$diag(1 \quad 5)$
$R_{washout,ground}$	$diag(3.09\times10^{-5} \quad 1.56\times10^{-4})$
$R_{washout,cruise}$	$diag(1.09\times10^{-5} \quad 1.56\times10^{-4})$
Q_e	1
Q_p	$diag(1 \quad 0.5)$

where the weighting matrices Q, R are now subscripted to indicated subsystems. Problems 2 and 3 represent two distinct implementations of a TEEM-based MPC. Both use a full state space model to avoid losing system information. The full state space model helps to explicitly account for constraints and transient operability goals in their optimal control problems. For the remainder of the paper, unless otherwise specified, the architectures described by Problems 2 and 3 are referred to as TEEM-CMPC and TEEM-DMPC respectively. When TEEM is not applied, $\tilde{y}_{TEEM}$ and $u_{washout}$ are removed from the cost functions and the prefix is dropped from the controllers. Similarly, TEEM-PI and PI refer to the benchmark PI architecture with and without TEEM implemented.

4. CASE STUDIES

The proposed MPC architectures are verified on a simulated burst-chop transient from low power to full power, represented in the AGTF30 system as the PLA change 48° to 80° to 48°. This is done at two environmental conditions: Ground (Alt = 5kft, MN = 0), with the burst starting at t = 10s and the chop starting at t = 25s; and Cruise (Alt = 40kft, MN = 0.8), with the burst starting at t = 30s and the chop starting at t = 80s. TEEM-MPC and MPC architectures are vetted against benchmark TEEM-PI and PI controllers. Note that the nominal acceleration and deceleration limiter schedules defined in [8] for the TEEM-PI and PI controllers are disabled in this study. Doing so provides a more accurate comparison to the MPC architectures. Weighting values and system parameters are presented in Table 1. MPC weights are manually tuned for an engine with TEEM applied. Weights for ground condition are tuned for a five-second rise time while weights for cruise condition are tuned to minimize N_{fan} trajectory error with respect to the burst throttle speed command. Note that the fuel flow component of the control weight matrix, $R(1,1)$ or R_e, is dependent on PLA and environmental conditions, leading to multiple gain values denoted as $R^{PLA}_{Environment}$ in Table 1. The gain schedule for the TEEM-PI motor controllers of [8] was designed with MATLAB's *pidtune* to reduce the stall margin overshoot during transients. The gains and schedule of the baseline fuel flow rate controller, discussed in [25], are tuned to provide desired thrust responsiveness and phase margin. Simulations are implemented in MATLAB using direct multiple shooting with CasADi, which includes the nonlinear optimization library iPOPT [30]. The sampling time is set to T_s = 0.02s and the time horizons are T = 0.1s and T_u = 0.04s. Closed-loop performance is evaluated using minimum SM, compressor map data, TSU, and TEI. Note that zero is the lowest possible value for the TSU metric as PR and PR_{SS} should be identical at the beginning and end of a transient. As a result, negative TSUs with a magnitude less than 0.1% were reported as zero in the data tables as values on this scale can be attributed to numerical errors in extracting the steady-state operating line for the environmental conditions. The MPC and TEEM-MPC constraint sets are:

$$
\begin{aligned}
\mathcal{X} &= \{0\text{rpm} \le N_{LPS} \le 7130\text{rpm}, 0\text{rpm} \le N_{HPS} \le 22500\text{rpm}\} \\
\mathcal{Y} &= \mathcal{Y}_f = \{0\text{rpm} \le N_{fan} \le 2300\text{rpm}, \\
&\qquad 0\text{rpm} \le N_{HPS} \le 22500\text{rpm}, \\
&\qquad |SM_{LPC}| \le \pm\inf, |SM_{HPC}| \le \pm\inf\} \\
\mathcal{U} &= \{W_{f,lb}(t)\text{pps} \le W_f \le W_{f,ub}(t)\text{pps}, \\
&\qquad -600\text{ft-lbf} \le M_{LPS} \le 0\text{ft-lbf}, \\
&\qquad 0\text{ft-lbf} \le M_{HPS} \le 200\text{ft-lbf}\}
\end{aligned}
$$

where the subscripts $\cdot_{lb}, \cdot_{ub}$ indicate lower and upper bounds. The time-varying fuel flow rate constraints are determined by the control limit constraints associated with shaft speed, pressure, or temperature at each time instant as defined in the AGTF30 model. The constraint $\pm\inf$ indicates an unconstrained parameter. Note the EM constraints are defined to restrict the LPS EM to power extraction and the HPS EM to power injection in accordance with the dual-spool strategy [8].

Figures 5 and 6 present the resultant LPC and HPC stall margins over time for the Ground scenario. Upon application of TEEM, the minimum stall margins are increased across each controller. The results presented in Table 2 confirm this observation, with all controllers increasing SM_{LPC} by ~2% and SM_{HPC} by

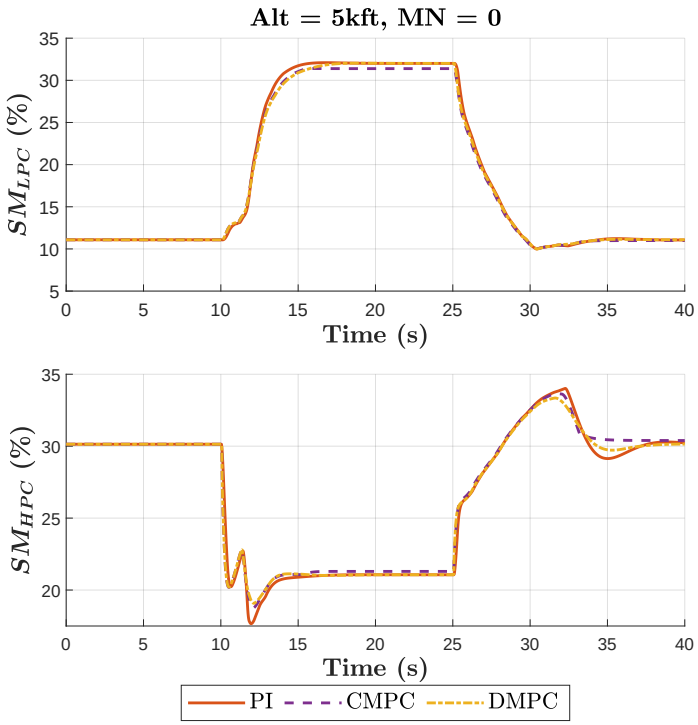

FIGURE 5: RESULTANT STALL MARGIN TRAJECTORIES ACROSS CONTROLLERS AT GROUND CONDITION WITHOUT TEEM APPLIED.

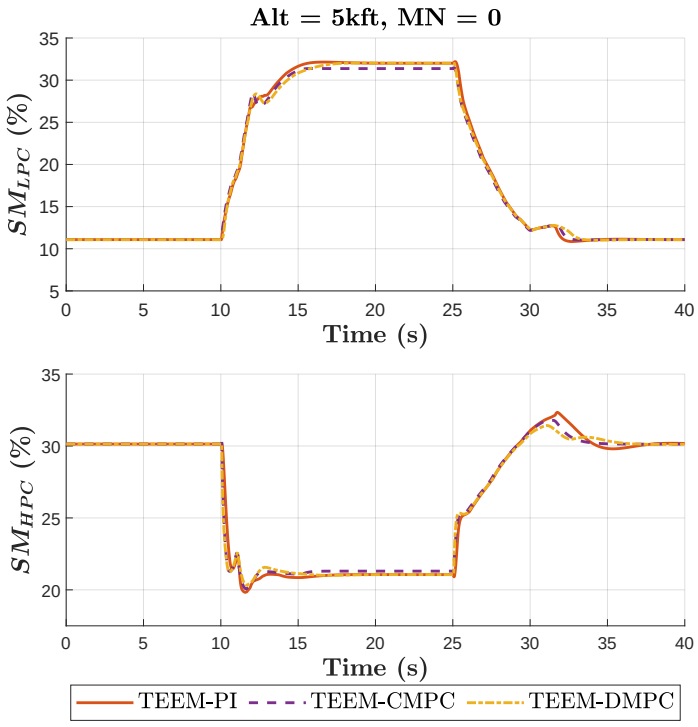

FIGURE 6: RESULTANT STALL MARGIN TRAJECTORIES ACROSS CONTROLLERS AT GROUND CONDITION WITH TEEM APPLIED.

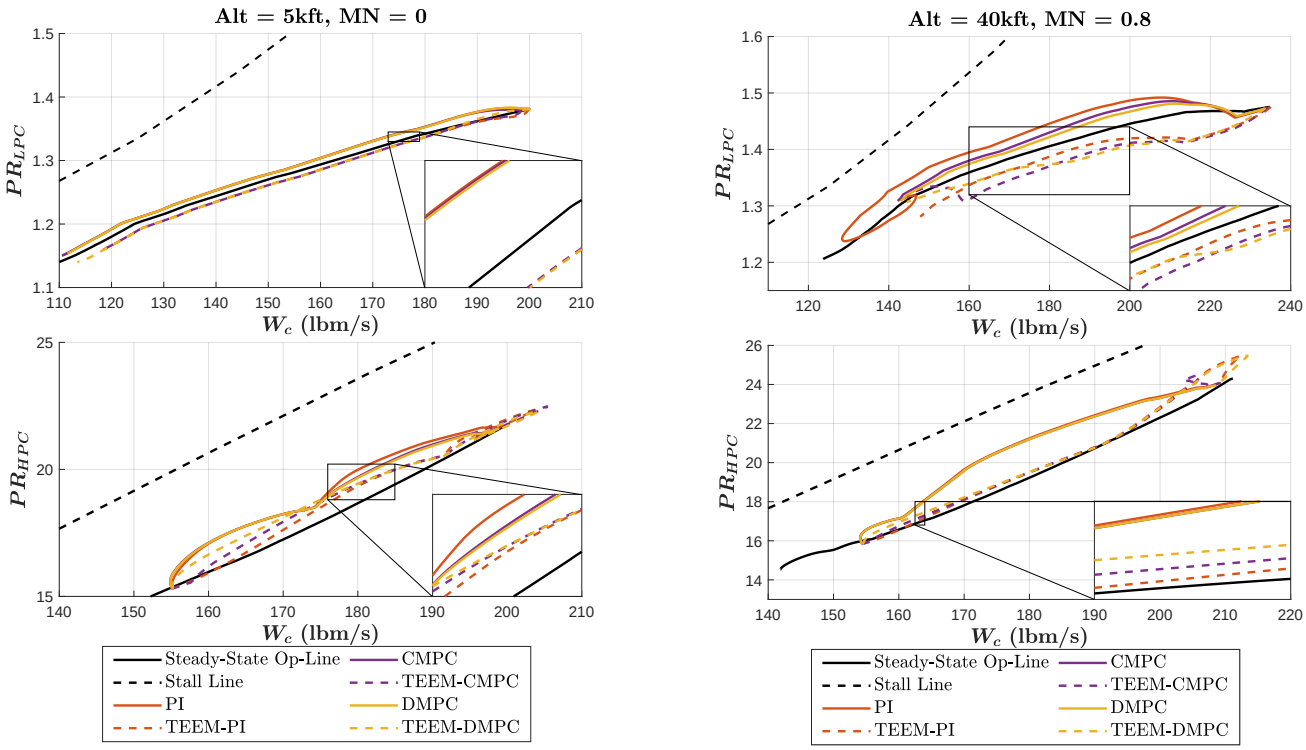

(a) Compressor map response at Ground condition.

(b) Compressor map response at Cruise condition.

FIGURE 7: LPC AND HPC COMPRESSOR MAP DATA ACROSS CONTROLLERS FOR GROUND (LEFT) AND CRUISE (RIGHT) CONDITIONS. DECELERATION SHOWN FOR LPC AND ACCELERATION SHOWN FOR HPC.

TABLE 2: RESULTS FOR GROUND CONDITION

	Min SM (%)		TEI		TSU (%)	
Controller	LPC	HPC	LPC	HPC	LPC	HPC
PI	10.0	17.7	0.721	2.37	9.31	26.9
CMPC	9.98	18.8	0.695	2.19	9.48	25.6
DMPC	10.0	19.1	0.697	2.14	9.38	25.6
TEEM-PI	12.2	19.8	0.485	0.861	0.153	13.7
TEEM-CMPC	12.2	20.1	0.478	1.17	0.0929	16.1
TEEM-DMPC	12.2	20.3	0.547	1.52	1.12	17.9

~1-2%. Figures 5 and 6 along with the data from Table 2 illustrate that the MPC and TEEM-MPC controllers maintain similar or larger minimum stall margins relative to the PI and TEEM-PI controls across both compressors. The HPC stall margin best demonstrates this, where the CMPC and DMPC maintain larger minimum SM_{HPC} values by ~1-2% compared to the PI. Figure 7 illustrates this result by presenting the resultant compressor map trajectories during deceleration for the LPC and during acceleration for the HPC. As seen in Fig. 7a, the TEEM-MPC HPC trajectories are pushed closer to the steady-state line than the TEEM-PI HPC trajectory. However, as indicated by the data, all controllers make similar gains from no TEEM to TEEM application, successfully shifting the transient running lines closer to or below the steady-state operating line. TEI and TSU results are also alike across controllers, decreasing in value when TEEM is

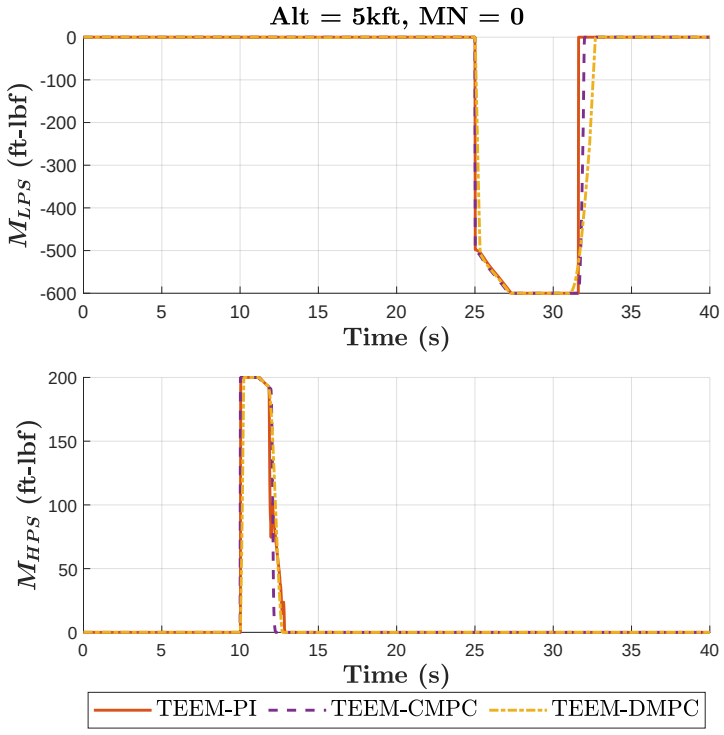

FIGURE 8: RESULTANT MOTOR TORQUE TRAJECTORIES ACROSS CONTROLLERS WITH TEEM IMPLEMENTED AT GROUND CONDITION.

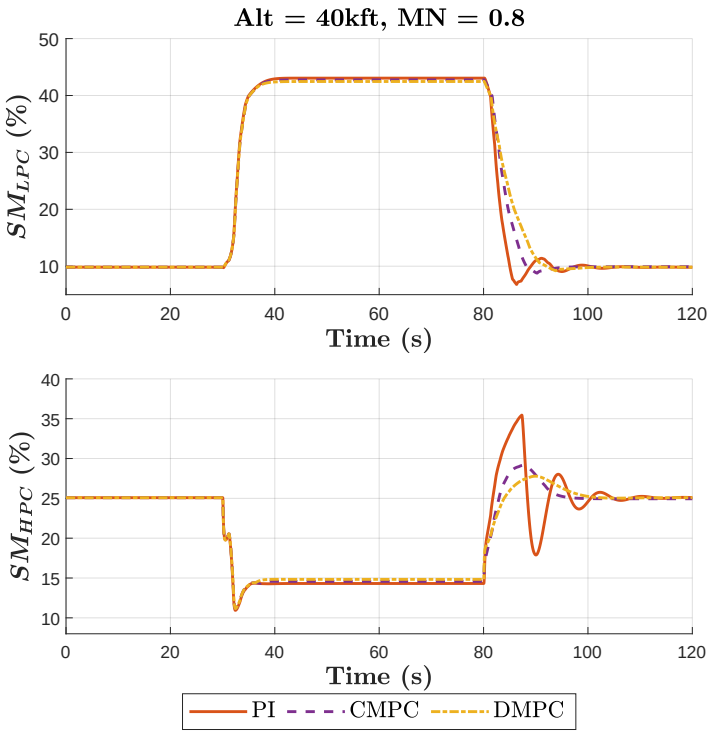

FIGURE 9: RESULTANT STALL MARGIN TRAJECTORIES ACROSS CONTROLLERS AT CRUISE CONDITION WITHOUT TEEM APPLIED.

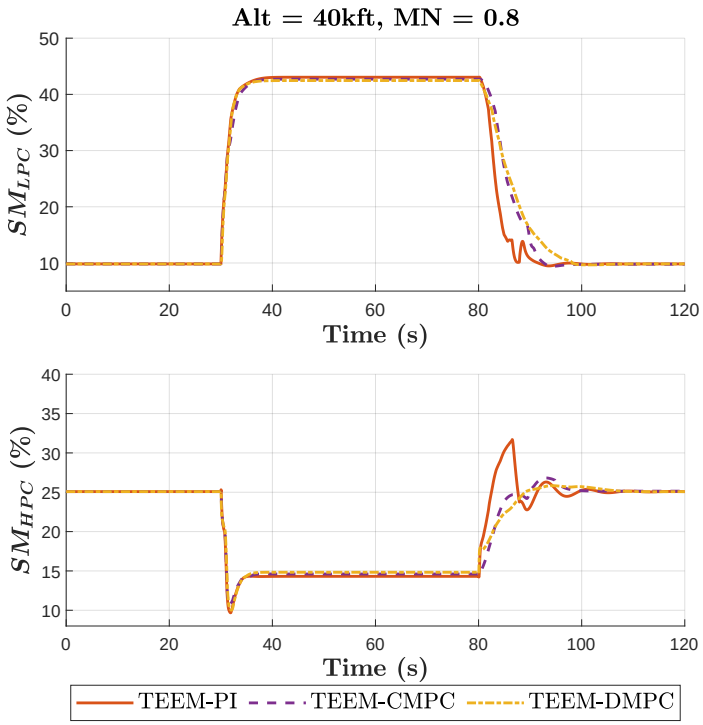

FIGURE 10: RESULTANT STALL MARGIN TRAJECTORIES ACROSS CONTROLLERS AT CRUISE CONDITION WITH TEEM APPLIED.

TABLE 3: RESULTS FOR CRUISE CONDITION

	Min SM (%)		TEI		TSU (%)	
Controller	LPC	HPC	LPC	HPC	LPC	HPC
PI	6.79	10.9	2.32	3.83	31.3	46.9
CMPC	8.79	11.2	1.30	3.72	14.0	46.1
DMPC	9.21	11.2	0.929	3.72	9.73	46.1
TEEM-PI	13.9	9.67	1.60	0.867	0.00	31.2
TEEM-CMPC	9.26	10.7	2.06	0.734	6.73	33.7
TEEM-DMPC	10.2	10.0	1.80	1.12	0.00	29.1

implemented. Although the TEEM-PI outperforms the TEEM-CMPC and TEEM-DMPC in HPC TEI and TSU reductions, the remaining data demonstrate comparable closed-loop controller performance both with and without TEEM. Figure 8 reveals the capabilities of the washout filter, which is able to activate and deactivate the motor torques in accordance with the system transient in a manner similar to the TEEM-PI. This demonstrates the advantage of the TEEM-MPC cost function, where desired control outcomes can be accounted for explicitly in one mathematical expression, thus simplifying the control design process.

The Cruise scenario controller performances are more diverse than the Ground scenario. Primarily, these results seem to reverse trends identified in the Ground condition. The data in Table 3 and the trajectories in Figs. 9 and 10 illustrate that, like the Ground scenario, all controllers have comparable transient stall margin trajectories and minimum stall margins. However, the outcome from applying TEEM is no longer consistently improved. For example, Fig. 10 shows that while SM_{LPC} improves when TEEM is applied, SM_{HPC} does not, reducing minimum

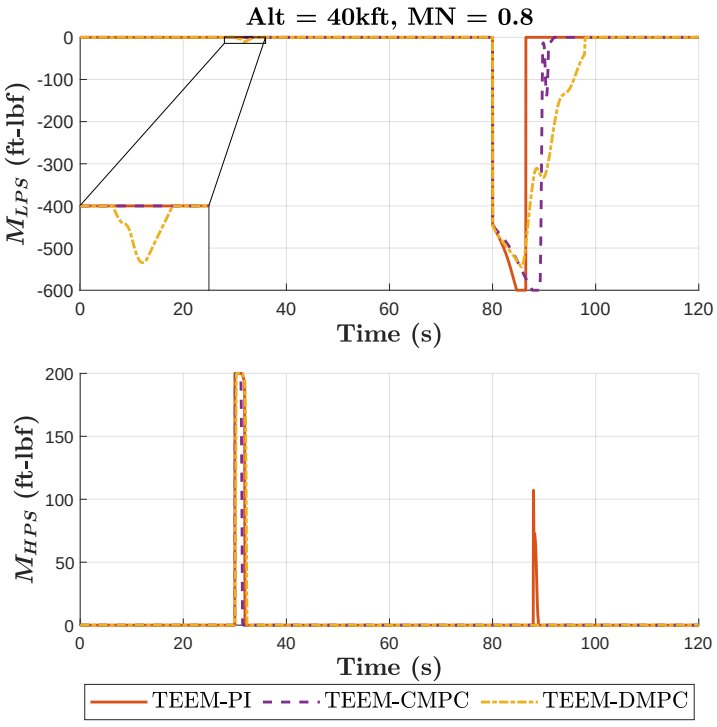

FIGURE 11: RESULTANT MOTOR TORQUE TRAJECTORIES ACROSS CONTROLLERS WITH TEEM IMPLEMENTED AT CRUISE CONDITION.

stall margins by ~1% across controllers. Additionally, the LPC TEI values for the TEEM-MPC controllers reported in Table 3 increase rather than decrease relative to the MPC controllers. This is in contrast to the TEEM-PI values which reduce in accordance with the TEEM concept. This phenomenon is explained through further investigation of the transient running lines displayed in Fig. 7b. Notice in Fig. 7b that the TEEM-MPCs' LPC trajectories move further below the steady-state operating line than the TEEM-PI. Recalling from Eq. (8) that TEI is an integral measure, this means that the further the distance of the transient running line from the steady-state operating line, the larger the TEI value. Thus, for example, when the HPC running lines are shifted very close to the steady-state line using TEEM, this results in the reduced values given in Table 3, matching the Ground condition trend. Further, when the LPC running lines are shifted far below the steady-state line using TEEM, this could result in values larger than the original amount without TEEM, which occurs in the TEI results for both MPCs and their TEEM counterparts. Therefore, although the TEI values increased with TEEM application, based on compressor stall line distance, the TEEM-MPC controllers are improving the transient operability akin to the TEEM-PI despite the degradation in TEI. Further improvements from applying TEEM are illustrated by the TSU values. For example, the resulting LPC and HPC TSUs show that each TEEM controller reduces the transient stack of the system, a desired TEEM outcome. TSU is reduced because the LPC and HPC transient running lines across controllers are pushed towards the steady-state operating line and thus away from the stall line, as shown in Fig. 7b. Thus, although the Cruise scenario results seem inconsistent with earlier trends, further investigation reveals that applying TEEM still achieves the desired transient operability improvements.

Torque trajectories (Fig. 11) at Cruise show that the washout filter correctly activates and deactivates the motors in accordance with the burst and chop, settling the motors once the system trajectories approach steady-state. However, Fig. 11 also highlights a potential disadvantage of the approach, apparent at ~30s where M_{LPS} briefly activates during the burst for the TEEM-DMPC (magnified in the figure). Because the TEEM-MPC controllers lack a transient indicator mechanism to manage the motor response, the controllers can command the motors at unexpected times. However, because this response occurs with TEEM-DMPC and not with TEEM-CMPC, it is possible this is a point of difference between the centralized and distributed approaches. The discrepancy should be further explored to determine if the difference is due to MPC architecture or poor gain selection for the TEEM-DMPC. The responses of the M_{HPS} trajectories highlight a potential advantage to using the washout filter in lieu of transient detection logic. The Benchmark TEEM-PI reactivates M_{HPS} at ~90s during deceleration, caused by an oscillation in the fan speed response as it attempts to resettle. The oscillations triggered the transient detection logic to mistakenly assume acceleration when the engine should be approaching steady-state. Oscillations could be prevented with improved tuning for the TEEM-PI, thus eliminating motor reactivation. The M_{HPS} responses of the TEEM-PI and TEEM-MPCs at ~90s suggest the washout filter is an advantageous alternative to detection logic. This is because fan speed oscillations do not trigger false transient identification, thus avoiding an undesired motor response.

5. CONCLUSIONS

This paper presented two applications of MPC to the TEEM control problem for hybrid-electric propulsion systems. Both approaches addressed set-point tracking, operating limits, and EM constraints within their cost functions, removing the need for additional control logic or schedules to account for various limiting conditions. By applying a constant-hold technique to handle control inputs, the MPCs were able to employ a full, linear state space model to thoroughly accommodate subsystem interactions. Additionally, a washout filter was used in the MPC design to penalize continuous use of the EMs. This allowed the MPCs to mimic the functionality of the transient on/off logic in the traditional closed-loop PI without an indicator function. Case studies highlighted that the MPCs increase minimum stall margin and reduce TEI and TSU to similar levels as the PI with and without the application of TEEM. While the TEI pattern seemed challenged in the Cruise case study, further analysis of the compressor maps revealed the MPCs achieved the desired transient operability outcome despite an increase in this metric. More significantly, results also highlighted that the washout filter was an effective replacement for transient detection logic, able to successfully activate and deactivate the motors in accordance with system transients and avoid false transient activation. Potential directions for future work include adding the VBV and VAFN as MPC control variables, incorporating energy storage components, testing other TEEM configurations, and executing hardware-in-the-loop testing.

ACKNOWLEDGMENTS

Elyse Hill's research was supported by an appointment to the NASA Postdoctoral Program at the NASA Glenn Research Center, administered by Oak Ridge Associated Universities under contract with NASA. This work was also supported by funding from the Power and Propulsion subproject under the Advanced Air Transport Technology Project as a part of the NASA Advanced Air Vehicles Program.

REFERENCES

[1] Pearce, Bob. "NASA Aeronautics Strategic Implementation Plan 2019 Update." (2019).

[2] Simon, Donald L., Connolly, Joseph W. and Culley, Dennis E. "Control Technology Needs for Electrified Aircraft Propulsion Systems." *Journal of Engineering for Gas Turbines and Power* Vol. 142 No. 1 (2020): pp. 1–10. DOI 10.1115/1.4044969.

[3] Schneider, Michael, Dickhoff, Jens, Kusterer, Karsten, Visser, Wilfried, Stumpf, Eike, Hofmann, Jan-Philipp and Bohn, Dieter. "Development of a Gas Turbine Concept for Electric Power Generation in a Commercial Hybrid Electric Aircraft." *Proceedings of the ASME Turbo Expo 2019: Turbomachinery Technical Conference and Exposition*. GT2019-92065. Phoenix, Arizona, June 17–21, 2019. DOI 10.1115/GT2019-92065. URL https://doi.org/10.1115/GT2019-92065.

[4] Richter, Hanz, Connolly, Joseph W. and Simon, Donald L. "Optimal Control and Energy Management for Hybrid Gas-Electric Propulsion." *Journal of Engineering for Gas Turbines and Power* Vol. 142 No. 9 (2020). DOI 10.1115/1.4047890.

[5] Sahoo, Smruti, Kavvalos, Mavroudis D., Diamantidou, Dimitra Eirini and Kyprianidis, Konstantinos G. "System-Level Assessment of a Partially Distributed Hybrid Electric Propulsion System." *Proceedings of the ASME Turbo Expo 2022: Turbomachinery Technical Conference and Exposition*. Rotterdam, Netherlands, June 17–21, 2022. American Society of Mechanical Engineers. DOI 10.1115/GT2022-81917. Accessed 2022-11-02, URL https://doi.org/10.1115/GT2022-81917.

[6] Papadopoulos, Konstantinos I., Nasoulis, Christos P., Ntouvelos, Elissaios G., Gkoutzamanis, Vasilis G. and Kalfas, Anestis I. "Power Flow Optimization for a Hybrid-Electric Propulsion System." *Journal of Engineering for Gas Turbines and Power* Vol. 144 No. 11 (2022). DOI 10.1115/1.4055478.

[7] Culley, Dennis E., Kratz, Jonathan L. and Thomas, George L. "Turbine Electrified Energy Management (TEEM) For Enabling More Efficient Engine Designs." *2018 Joint Propulsion Conference*. AIAA 2018-4798. Cincinnati, OH, July 9–11, 2018. DOI 10.2514/6.2018-4798. URL https://doi.org/10.2514/6.2018-4798.

[8] Kratz, Jonathan L., Culley, Dennis E. and Thomas, George L. "A Control Strategy for Turbine Electrified Energy Management." *AIAA Propulsion and Energy 2019 Forum*. AIAA 2019-4499. Indianapolis, IN, August 19–22, 2019. DOI 10.2514/6.2019-4499. URL https://doi.org/10.2514/6.2019-4499.

[9] Kratz, Jonathan L., Culley, Dennis E. and Thomas, George L. "Evaluation of Electrical System Requirements for Implementing Turbine Electrified Energy Management." *AIAA Propulsion and Energy 2019 Forum*. AIAA 2019-4502. Indianapolis, IN, August 19–22, 2019. DOI 10.2514/6.2019-4502. URL https://doi.org/10.2514/6.2019-4502.

[10] Kratz, Jonathan L. and Simon, Donald. "Failure Modes and Mitigation Strategies for a Turboelectric Aircraft Concept with Turbine Electrified Energy Management." *AIAA SciTech 2022 Forum*. AIAA 2022-1191. San Diego, CA, January 3–7, 2022. DOI 10.2514/6.2022-1191. URL https://doi.org/10.2514/6.2022-1191.

[11] Kratz, Jonathan L. and Culley, Dennis E. "Enhancement of a Conceptual Hybrid Electric Tilt-Wing Propulsion System through Application of the Turbine Electrified Energy Management Concept." *AIAA SciTech 2021 Forum*. AIAA 2021-0875. Virtual, Online, January 11–15, 2021. DOI 10.2514/6.2021-0875. URL https://doi.org/10.2514/6.2021-0875.

[12] Kratz, Jonathan, Connolly, Joseph, Amthor, Aria, Buescher, Halle, Bianco, Santino and Culley, Dennis. "Turbine Electrified Energy Management for Single Aisle Aircraft." *2022 IEEE Transportation Electrification Conference & Expo (ITEC)*: pp. 658–663. Anaheim, CA, June 15–17, 2022. DOI 10.1109/ITEC53557.2022.9813818. URL https://doi.org/10.1109/ITEC53557.2022.9813818.

[13] Kratz, Jonathan. "Transient Optimization of a Gas Turbine Engine." *AIAA SciTech 2023 Forum*. AIAA 2023-0703. National Harbor, MD, USA, January 23–27, 2023. DOI 10.2514/6.2023-0703. URL https://doi.org/10.2514/6.2023-0703.

[14] Rawlings, James B. and Mayne, David Q. *Model Predictive Control: Theory and Design*, 2nd ed. Nob Hill Publishing, Madison (2009).

[15] Seok, Jinwoo, Kolmanovsky, Ilya and Girard, Anouck. "Integrated/coordinated control of aircraft gas turbine engine and electrical power system: Towards large electrical load handling." *2016 IEEE 55th Conference on Decision and Control (CDC)*: pp. 3183–3189. Las Vegas, NV, December 12–14, 2016. DOI 10.1109/CDC.2016.7798747. URL https://doi.org/10.1109/CDC.2016.7798747.

[16] Seok, Jinwoo, Kolmanovsky, Ilya and Girard, Anouck. "Coordinated Model Predictive Control of Aircraft Gas Turbine Engine and Power System." *Journal of Guidance, Control, and Dynamics* Vol. 40 No. 10 (2017): pp. 2538–2555. DOI 10.2514/1.G002562.

[17] Dunham, William, Hencey, Brandon, Kolmanovsky, Ilya and Girard, Anouck. "Predictive propulsion and power control for large transient power loads in a More Electric Aircraft." *2017 American Control Conference (ACC)*: pp. 4055–4061. Seattle, WA, May 24–26, 2017. DOI 10.23919/ACC.2017.7963577. URL https://doi.org/10.23919/ACC.2017.7963577. ISSN: 2378-5861.

[18] Seok, Jinwoo, Reed, David M., Kolmanovsky, Ilya V. and Girard, Anouck R. "Coordinated Model Predictive Control of Aircraft Gas Turbine Engine with Simplified Electrical System Model." *2018 Annual American Control Conference (ACC)*: pp. 1460–1466. Milwaukee, WI, June 27–29, 2018. DOI 10.23919/ACC.2018.8431504. URL https://doi.org/10.23919/ACC.2018.8431504.

[19] Dunham, William, Hencey, Brandon, Kolmanovsky, Ilya and Girard, Anouck. "Scenario Based Stochastic MPC for More Electric Aircraft Coordinated Engine and Power Management." *2019 American Control Conference (ACC)*: pp. 4223–4228. Philadelphia, PA, July 10–12, 2019. DOI 10.23919/ACC.2019.8814639. URL https://doi.org/10.23919/ACC.2019.8814639. ISSN: 2378-5861.

[20] Doff-Sotta, Martin, Cannon, Mark and Bacic, Marko. "Optimal energy management for hybrid electric aircraft." *IFAC-PapersOnLine* Vol. 53 No. 2 (2020): pp. 6043–6049. DOI 10.1016/j.ifacol.2020.12.1672.

[21] Almeida, Fabio. "Management of Electrical Power Generation on Gas Turbine with Model Predictive Control." *AIAA SciTech 2022 Forum*. AIAA 2022-0444. San Diego, CA, January 3–7, 2022. DOI 10.2514/6.2022-0444. URL https://doi.org/10.2514/6.2022-0444.

[22] Dunham, William, Hencey, Brandon, Girard, Anouck R. and Kolmanovsky, Ilya. "Distributed Model Predictive Control for More Electric Aircraft Subsystems Operating at Multiple Time Scales." *IEEE Transactions on Control*

Systems Technology Vol. 28 No. 6 (2020): pp. 2177–2190. DOI 10.1109/TCST.2019.2932654.

[23] Jiang, Zhenhua and Pakmehr, Mehrdad. "Model Predictive Control for Distributed Electric Propulsion of eVTOL Vehicles: A Preliminary Design." *AIAA SciTech 2022 Forum*. AIAA 2022-0878. San Diego, CA, January 3–7, 2022. DOI 10.2514/6.2022-0878. URL https://doi.org/10.2514/6.2022-0878.

[24] Negenborn, R.R. and Maestre, J.M. "Distributed Model Predictive Control: An Overview and Roadmap of Future Research Opportunities." *IEEE Control Systems Magazine* Vol. 34 No. 4 (2014): pp. 87–97. DOI 10.1109/MCS.2014.2320397.

[25] Chapman, Jeffryes W. and Litt, Jonathan S. "Control Design for an Advanced Geared Turbofan Engine." *53rd AIAA/SAE/ASEE Joint Propulsion Conference*. AIAA 2017-4820. Atlanta, GA, USA, July 10–12, 2017. DOI 10.2514/6.2017-4820. URL https://arc.aiaa.org/doi/10.2514/6.2017-4820.

[26] Chapman, Jeffryes W., Lavelle, Thomas M., May, Ryan D., Litt, Jonathan S. and Guo, Ten-Huei. "Toolbox for the Modeling and Analysis of Thermodynamic Systems (T-MATS) User's Guide." Technical Report No. NASA/TM-2014-216638. NASA, Cleveland, OH. 2014. URL https://ntrs.nasa.gov/citations/20140012486.

[27] Chapman, Jeffryes W. and Litt, Jonathan S. "An Approach for Utilizing Power Flow Modeling for Simulations of Hybrid Electric Propulsion Systems." *2018 AIAA/IEEE Electric Aircraft Technologies Symposium (EATS)*. AIAA 2018-5018. Cincinnati, OH, July 9–11, 2018. DOI 10.2514/6.2018-5018. URL https://doi.org/10.2514/6.2018-5018.

[28] Kratz, Culley Dennis E. Lehan Julian, Jonathan L. "Transient Optimization for the Betterment of Turbine Electrified Energy Management." *AIAA SciTech 2023 Forum*. AIAA 2023-0704. National Harbor, MD, USA, January 23–27, 2023. DOI 10.2514/6.2023-0704. URL https://doi.org/10.2514/6.2023-0704.

[29] Haley, P. and Soloway, D. "Experimental validation of generalized predictive control for active flutter suppression." *Proceeding of the 1996 IEEE International Conference on Control Applications*: pp. 125–129. Dearborn, MI, September 15–November 18, 1996. DOI 10.1109/CCA.1996.558618. URL https://doi.org/10.1109/CCA.1996.558618.

[30] Andersson, Joel A. E., Gillis, Joris, Horn, Greg, Rawlings, James B. and Diehl, Moritz. "CasADi: a software framework for nonlinear optimization and optimal control." *Mathematical Programming Computation* Vol. 11 No. 1 (2019): pp. 1–36. DOI 10.1007/s12532-018-0139-4.